Italian Journal of Engineering Geology and Environment
www.ijege.uniroma1.it

NUMERICAL MODELLING OR CONVENTIONAL ANALYSES? WHEN AN INTEGRATED APPROACH BECOMES FUNDAMENTAL IN UNDERSTANDING SLOPE FAILURE MECHANISMS

Mariagiulia ANNIBALI CORONA(*), Francesco OTTAVIANI(*), Marco FRANCESCHETTI(*), Filippo INVERNIZZI(**) & Mirko FRANCIONI(*)

(*)Università degli Studi 'Carlo Bo' di Urbino - Dipartimento di Scienze Pure e Applicate (DISPeA) - Urbino, Italy
(**)Parco Regionale del Conero - Sirolo, Italy
Corresponding author: mariagiulia.annibalicorona@uniurb.it

EXTENDED ABSTRACT

Gli ambienti costieri rocciosi rappresentano sistemi geomorfologici altamente dinamici, nei quali la stabilità dei versanti è controllata dall'interazione tra assetto geologico, anisotropia meccanica dell'ammasso roccioso e processi di origine marina. La difficoltà di accesso alle falesie costiere ad alto sviluppo verticale costituisce un ulteriore elemento di complessità nello studio diretto di tali contesti.

I recenti sviluppi nelle tecniche di telerilevamento hanno tuttavia consentito significativi avanzamenti nell'analisi di queste aree costiere difficilmente accessibili. L'impiego integrato di laser scanner terrestre e da drone, fotogrammetria da UAV e dati multisorgente permette ricostruzioni tridimensionali ad alta risoluzione della geometria del versante e delle reti di discontinuità, fornendo una base robusta per analisi strutturali e cinematiche dettagliate.

Il presente studio adotta un approccio metodologico integrato per l'analisi della stabilità dei versanti nel settore costiero del Monte Conero (Italia centrale), con particolare riferimento alla falesia di Piangrande, caratterizzata da un fronte elevato e ripido che sovrasta infrastrutture turistiche. La limitata accessibilità del sito ha richiesto un utilizzo estensivo della fotogrammetria da UAV e di modelli digitali del terreno derivati da rilievi LiDAR per la ricostruzione della geometria del versante e dei principali assetti strutturali. Le acquisizioni fotogrammetriche frontali e oblique si sono rivelate essenziali per la rappresentazione accurata delle porzioni geometricamente più complesse del versante, mentre i dati LiDAR, acquisiti con geometria prevalentemente nadirale, hanno fornito un inquadramento topografico di scala generale. I dati di telerilevamento sono stati integrati con rilievi geologico-tecnici dettagliati condotti nei settori accessibili, caratterizzati dal medesimo assetto litologico e strutturale, consentendo la validazione delle interpretazioni remote. L'analisi integrata ha permesso di individuare un piano di stratificazione a basso angolo di immersione (S0), associato a tre sistemi di fratture ad alto angolo (J1-J3), che definiscono un ammasso roccioso anisotropo e strutturalmente complesso. Sono state inoltre riconosciute evidenze di instabilità pregresse e settori potenzialmente instabili lungo la falesia.

Al fine di simulare i dissesti storici e valutare la stabilità dei settori critici, sono state eseguite analisi cinematiche, di equilibrio limite e numeriche. Le analisi cinematiche stereografiche indicano che i meccanismi di scivolamento planare e a cuneo rivestono un ruolo secondario, mentre il ribaltamento flessurale rappresenta il meccanismo di instabilità prevalente. Le analisi all'equilibrio limite e di modellazione numerica sono state condotte su modelli derivati sia da dati LiDAR sia fotogrammetrici. Entrambe le analisi hanno mostrato una stabilità globale del versante quando si utilizza il modello LiDAR e cedimenti localizzati quando viene considerato il modello fotogrammetrico. In quest'ultimo caso, i cedimenti sono localizzati in aree di versante ad elevata inclinazione o addirittura sospese che non erano state ricostruite dal rilievo LiDAR. Tali risultati concordano solo in parte con quanto evidenziato dai dettagliati rilievi geologici e geomorfologici e dall'interpretazione (effettuata anche tramite tecniche di realtà virtuale e aumentata) dei dati telerilevati, dove si evidenzia la presenza di cinematismi simili a quelli mostrati dalle analisi all'equilibrio limite e modellazioni numeriche, ma anche cinematici più complessi ed estesi e legati alla propagazione della fratturazione lungo il versante.

Nel complesso, lo studio evidenzia come i metodi analitici e numerici, pur fondamentali, possano non essere sufficienti a rappresentare tutta la complessità dei processi di instabilità che interessano le falesie costiere rocciose. Le tecniche di telerilevamento costituiscono strumenti essenziali per la ricostruzione geometrica e strutturale, ma la loro interpretazione deve essere inserita in un solido quadro geologico. Un approccio integrato rimane pertanto indispensabile per una valutazione affidabile della pericolosità dei versanti rocciosi costieri.

IJEGE, Special Issue 1, (2026): 5-15, DOI: 10.4408/IJEGE.2026-01.S-01
E-ISSN 2035-5688 | ISSN 1825-6635 / ©Author(s)

ABSTRACT

Conventional kinematic and limit equilibrium analyses represent fundamental tools for slope stability assessment, especially under relatively simple geological and geometrical conditions. In structurally complex rock slopes, however, these approaches may be insufficient to fully describe failure kinematics, making integration with numerical modelling necessary. This study presents an integrated methodological framework combining conventional analyses and numerical modelling, applied to the Monte Conero coastal sector (Ancona, central Italy), an area characterized by a highly complex structural setting and significant exposure to rockfall and toppling hazards. Engineering geological and geomorphological surveys were combined with UAV-based photogrammetry and LiDAR to reconstruct slope geometry and discontinuity networks, providing the basis for kinematic and limit equilibrium analyses. While these methods allowed the identification of potential instability mechanisms, they were unable to fully reproduce deformation patterns observed in the field. Numerical modelling was therefore applied to simulate different geological and mechanical scenarios, enabling a more realistic representation of slope behaviour and failure mechanisms. The results highlight both the capabilities and the limitations of numerical approaches, underlining the importance of careful model calibration, validation and critical interpretation. Overall, the study demonstrates that an integrated analytical and numerical approach is essential for reliable slope stability assessment in structurally complex coastal environments and, at the same time, that geological interpretation remains the key component of any engineering geological assessment.

Keywords: *rock slope instability, photogrammetry, LiDAR, numerical modelling*

INTRODUCTION

High coastal cliffs constitute a large portion of the world's shorelines and are inherently prone to instability due to their structural complexity and the coexistence of contrasting lithologies (Williams & Pranzini, 2018; Young & Carilli, 2019). Large-scale discontinuities, including bedding planes, faults, and inherited structural fabrics, exert a primary control on rock mass behaviour and strongly predispose slopes to structurally controlled failure mechanisms (Weidinger *et alii*, 2014; Agliardi *et alii*, 2019; Fan *et alii*, 2019; Guerriero *et alii*, 2024). These conditions are further aggravated by anthropogenic pressures and climate-driven processes such as increased storm activity, wave action, and sea-level rise, which enhance coastal erosion and instability (Fullin *et alii*, 2023; Feliziani *et alii*, 2024).

Discontinuity networks govern cliff morphology, failure kinematics, and groundwater circulation, with elevated pore-water pressures along low-strength planes acting as key triggering factors for rock-slope failures (Neuman, 2005). Although conventional kinematic and limit equilibrium methods are widely used for preliminary stability assessment, their applicability is limited in highly fractured and structurally complex rock masses. In such settings, numerical modelling approaches can provide additional insights into stress redistribution and failure evolution, provided they are supported by an accurate geological characterization.

Recent advances in remote sensing have significantly improved the investigation of steep and inaccessible coastal cliffs. UAV-based photogrammetry and LiDAR enable the generation of high-resolution three-dimensional models for detailed structural analysis (Westoby *et alii*, 2012; Esposito *et alii*, 2017). More recently, portable tablet-based LiDAR systems have emerged as effective tools for rapid close-range surveys, while augmented and virtual reality (AR/VR) environments offer new possibilities for immersive visualization and interpretation of complex geological datasets.

Within this framework, this study applies an integrated approach based on remote sensing, conventional analyses and numerical modelling to the Monte Conero coastal slope (central Italy), with particular focus on the Piangrande Cliff. This sector is characterized by pronounced structural complexity and hosts tourist infrastructure and accommodation facilities at the slope toe, making it particularly vulnerable to rockfall and toppling hazards. Due to the limited accessibility of large portions of the cliff, remote sensing techniques were extensively employed to reconstruct slope geometry and discontinuity patterns. To support and validate these interpretations, additional surveys were conducted at two accessible sites within the same geological setting, Poggio Quarry and Riparo dello Speco.

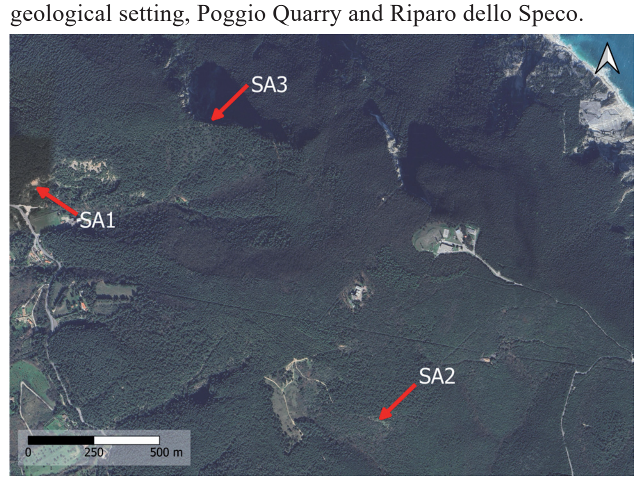

Fig. 1 - Geographical location of the study area within the Conero Regional Park (Ancona, Italy), showing the three surveyed sites. Arrows indicate the position of the investigated areas: Survey area 1 (SA1), Poggio Quarry; Survey area 2 (SA2), Riparo dello Speco; Survey area 3 (SA3), Piangrande Cliff

The combined use of remote sensing and field-based observations provided a comprehensive dataset for structural characterization, kinematic and limit equilibrium analyses, and numerical modelling of slope behaviour. The location of the investigated sites is shown in Figure 1.

STUDY AREA: GEOLOGICAL AND GEOGRAPHICAL SETTING

The Portonovo sector of the Conero Promontory represents one of the most fragile and landslide-prone coastal systems in the central Adriatic. Historical records and geological evidence document recurrent small and large-scale slope failures affecting the Portonovo littoral zone since at least the Medieval period. Radiocarbon analyses have confirmed the age of these events, highlighting the long-term geomorphological instability of this seismically active high-coast sector (Montanari *et alii*, 2016).

From a geological standpoint, the Conero Promontory belongs to the foredeep–foreland system of the Outer Northern Apennines (Calamita *et alii*, 1999; Cello & Coppola, 1989). Monte Conero is structured as an open NE-verging asymmetric anticline intersected by E–W strike-slip faults, with the NE limb dipping 70–85° and the SW limb dipping approximately 20° (Cello & Coppola, 1989; Pierantoni *et alii*, 2013). The geological formations outcropping in the promontory belong to the Umbria-Marche stratigraphic succession and range from Cretaceous to the Pliocene (Coltorti & Sarti, 2011; Montanari *et alii*, 2016). More specifically, the Piangrande area is characterized by Eocene marly limestones (Scaglia Rossa Fm.).

Across the different sectors of the promontory, instability phenomena include composite movements, rotational slides, rockfalls and block toppling. In the study area, these are controlled by structural discontinuities, such as bedding planes, faults, joints, and inherited folding fabrics, which promote planar, wedge, and toppling failure mechanisms.

Three representative survey sites within the Scaglia Rossa Fm. were selected to investigate rock mass characteristics and morphological conditions. Survey Area 1 (SA1, Poggio Quarry) is an abandoned quarry where well-exposed rock outcrops. Survey Area 2 (SA2, Riparo dello Speco) is located along the mid-slope of a southeast-facing cliff sector and was recently discovered by Dr. Filippo Invernizzi (Parco Regionale del Conero). Survey Area 3 (SA3, the Piangrande Cliff) represents the main focus area of the study, encompassing an extensive coastal cliff sector affected by pronounced structural complexity and active instability processes. Due to the inaccessibility of the cliff, SA3 is the only site investigated exclusively through remote sensing techniques.

MATERIAL AND METHODS

Geomechanical and Remote Sensing surveys

Conventional geomechanical scanlines were carried out in the accessible sites SA1 and SA2. To improve data interpretation, all sites were also investigated using remote sensing techniques. The DJI Mavic 3E drone was used to conduct UAV photogrammetric surveys at SA1 and SA3. The UAV was equipped with a 4/3 CMOS sensor with 20 MP effective resolution and a field of view of 84°. The camera aperture ranges from f/2.8 to f/11, the focus distance from 1 m to infinity, and the ISO sensitivity from 100 to 6400. The surveys were undertaken in manual mode with approximately 80% side and frontal overlap between consecutive photographs. The acquired images were processed using the Structure-from-Motion (SfM) software Agisoft Metashape (Agisoft, 2025). This tool allows the generation of point clouds, 3D models, orthophotos and Digital Surface Models from images. At SA2 (Riparo dello Speco), the conventional geomechanical survey was integrated with a LiDAR survey performed using an iPad Pro (equipped with a LiDAR sensor which uses laser pulses to measure the distance of objects up to about 5 meters). The estimated precision of the iPad LiDAR is around 2 cm for a single pass (Atencio *et alii*, 2024). A drop in accuracy has been noted when scanning small, complex objects, but good performance has been observed when capturing large objects and walls (Łabędź *et alii*, 2022), as in the present case. The cave was scanned with multiple passes, starting from the entrance and taking care to cover the entire internal surface of the cave. Geomechanical characterization of the 3D models (from UAV and iPad) was performed by extracting dip and dip direction measurements using the Plane and Trace tool (Cloudcompare Team, 2025) available in the Compass Plug-in in CloudCompare (Girardeau-Montaut, 2006).

Geomorphological analyses and geomechanical characterization

The methodological framework adopted in this study is based on the integration of conventional geomorphological and geomechanical investigations with remote sensing techniques, to characterize slope instability processes in structurally complex coastal environments. The approach was applied to the Monte Conero coastal slope, with a particular focus on the Piangrande Cliff, while two additional sites (SA1 and SA2) were investigated as complementary areas to support structural interpretation, calibration, and validation of the analyses. Geomorphological investigations were conducted to identify slope morphology, evidence of active and relict instability phenomena, and the spatial distribution of erosional and depositional landforms. These observations provided the contextual framework for subsequent geomechanical characterization and stability analyses. Geomechanical surveys were carried out following ISRM recommendations (ISRM, 1978), including lithological description, rock mass characterization, and systematic measurement of discontinuity sets using scanline techniques. Where direct access to rock outcrops was possible, discontinuity orientation, spacing, persistence, roughness, aperture, and infilling were measured in situ.

In sectors characterized by partial or total inaccessibility, particularly along steep coastal cliffs, geomechanical characterization was supported by remote sensing data, enabling the reconstruction of three-dimensional virtual outcrop models.

The integration of conventional field measurements with photogrammetric models ensured spatial continuity of the structural dataset and reduced bias associated with localized or anthropogenic features, such as those related to former quarrying activities. Structural and geometrical parameters derived from both direct and remote surveys were combined into a unified geomechanical dataset, forming the basis for kinematic analyses, conventional slope stability assessments, and subsequent numerical modelling.

Kinematic analyses

Kinematic analyses were carried out to evaluate potential failure mechanisms at the Piangrande Cliff based on the orientation of rock discontinuities relative to slope geometry. Structural data acquired from field scanlines, UAV-derived models and tablet-based LiDAR datasets were integrated to ensure spatial continuity across all survey areas.

The orientation and spacing of discontinuities were projected onto stereonets using DIPS software, following the Markland stereographic method and its subsequent operational developments, to identify zones susceptible to kinematically admissible movements. The analysis considered planar sliding along single discontinuities, wedge sliding resulting from the intersection of two planes, and both direct and flexural toppling of rock columns. These analyses provide a geometrically based assessment of potential instability, highlighting sectors of the slopes where the relative orientation of joints and slope faces could favour detachment of rock blocks.

The kinematic analysis was particularly relevant for the Piangrande Cliff, where inaccessibility and complex structural patterns limited the applicability of conventional in situ surveys. Data from SA1 and SA2 served to validate the stereographic interpretation and to support extrapolation of structural features to less accessible cliff sectors.

Limit equilibrium analysis

Two models of SA3 (Piangrande Cliff), derived respectively from UAV-LiDAR and UAV-photogrammetry data, were processed using the same MATLAB-based workflow and subsequently refined in Rhinoceros using the Griddle plug-in before being imported into RocSlope3 (Rocscience, 2023). Only two joint families were considered due to the computational limitations of the hardware available for this phase. For the same reason, it was not possible to use the actual spacing of the joint families; instead, a spacing of 2 meters was used for all discontinuities. This simplification may affect the size and frequency of potentially unstable blocks and therefore introduces some uncertainty in the quantitative results; however, it is unlikely to significantly affect the identification of the main instability mechanisms controlled by the dominant structural sets.

The software evaluates the kinematic feasibility of rock block movement based on the geometry and orientation of the discontinuities. This step is essential for assessing the potential hazard to structures located downstream.

Numerical modelling

Numerical modelling was performed on two different 2D sections extracted from the LiDAR- and photogrammetry-based models (Fig. 2). The sections were extracted using a MATLAB tool specifically developed for this purpose. The sections were handled as STL surfaces and refined in Rhinoceros using the Griddle plug-in prior to import into the 3DEC numerical code. Discontinuity sets were included based on the results of the kinematic analysis.

In this work, the Mohr–Coulomb constitutive model was adopted to simulate the mechanical behaviour of the rock mass and to calculate the displacements of the blocks forming the slope. The mechanical parameters used in the model were derived from previous geomechanical studies (Martin *et alii*, 2020) and calibrated using the results of recent field surveys (Mandaglio *et alii*, 2024). A friction angle of 45° was assigned to the intact rock mass, while a reduced value of 35° was adopted for discontinuities, consistent with the values measured during the geomechanical survey. Cohesion was assumed equal to 0 kPa for bedding planes and joints, whereas a cohesion value of 6.75×10^5 Pa was assigned to the rock mass.

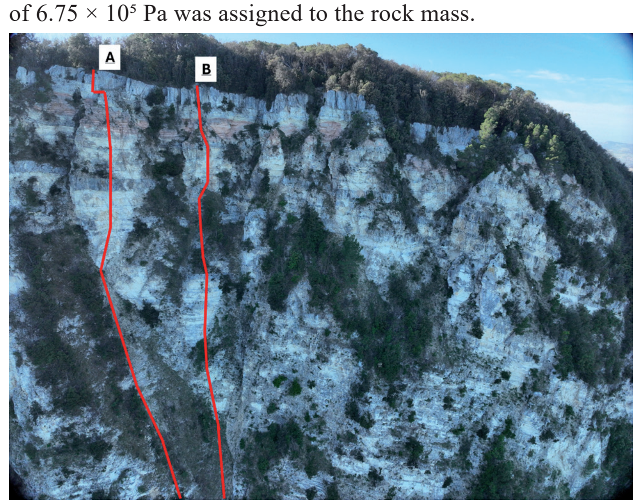

Fig. 2 - Survey Area 3 (SA3), Piangrande Cliff: Section 1 (A) and Section 2 (B)

RESULTS

To create a photogrammetric model of SA1, 622 images were collected during the UAV survey. The final product (Fig. 3a) consists of a 3D object with 19,503,418 faces and 100,004,036

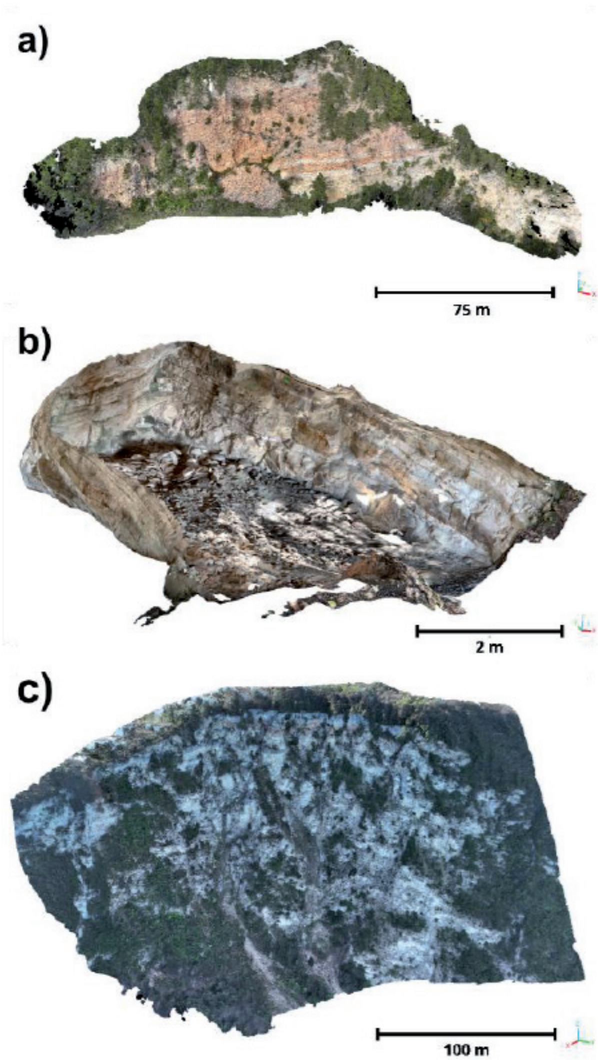

Fig. 3 - 3D models of the investigated sites: (a) UAV-photogrammetric model of Poggio Quarry (SA1); (b) iPad-based LiDAR model of Riparo dello Speco (SA2); (c) UAV-photogrammetric model of Piangrande Cliff (SA3)

points. The iPad-based LiDAR model of SA2 (Fig. 3b) consists of a 3D object with a mesh of 129,746 faces and 100,000,016 points. In SA3, both LiDAR and photogrammetric UAV surveys were performed. During the UAV-LiDAR survey, 1,827 LiDAR acquisition frames were collected, and a DTM with a 0.5 × 0.5 m resolution was generated. During the UAV photogrammetry survey, 715 photographs were acquired. Agisoft Metashape software was used to create a 3D model of the slope. The final product (Fig. 3c) consists of 3,075,528 faces and 161,657,934 points.

The stereographic projections shown in Figure 4 summarize the orientation data of discontinuities measured at the three investigated survey areas: SA1 (Figure 4a), SA2 (Figure 4b), and SA3 (Figure 4c). The stereonets highlight marked differences in data density and cluster definition, reflecting variations in outcrop size, exposure conditions, and sampling representativeness.

Among the investigated outcrops, SA3 (Figure 3c) represents the most extensive and structurally representative site. The large number of measurements (308 poles) and the homogeneous exposure of the rock mass allow a robust identification of four main discontinuity sets, including one bedding-related set (S0) and three joint sets (J1, J2, and J3).

In contrast, the stereonets of SA1 (Figure 4a) and SA2 (Figure 4b) show a lower number of measurements and a more scattered distribution of poles. At SA1, the bedding plane (S0) and two joint sets (J1 and J2) are clearly recognizable, whereas the J3 set is weakly expressed and poorly clustered. The SA2 outcrop is dominated by a single, well-defined cluster corresponding to a steeply dipping joint set, while the remaining sets are either poorly represented or not clearly distinguishable. These differences, together with the slight rotation of the identified clusters, are interpreted as the effect of local structural conditions, limited exposure, and sampling constraints.

The geomechanical characterization of the identified discontinuity sets is summarized in Table 1. The bedding plane (S0) exhibits close spacing at the decimetric scale (approximately 0.1 m), moderate surface weathering, rough surface conditions, and relatively large apertures, reaching up to 5.0 mm. The infilling material is non-cohesive, and discontinuities were observed to be dry during field surveys. Joint sets J1, J2, and J3 are characterized by steep dips and mean spacing values ranging between 0.1 and 0.2 m, indicating a moderate joint density within the rock mass. Persistence varies significantly among the joint sets, with J3 showing the highest persistence (up to 2.1 m), while J1 and J2 display shorter trace lengths of approximately 0.6 m and 0.3 m, respectively. Joint apertures range from 1.2

Par.	S0	J1	J2	J3
Type	Bed	J	J	J
Dip (°)	18	88	87	88
Dip dir. (°)	235	050	116	003
Pers. (m)	–	0.6	0.3	2.1
Spac. (m)	0.1	0.2	0.2	0.1
Aper. (mm)	5.0	1.2	2.5	3.0
Fill.	NC	NC	NC	NC
Weath.	MW	SW	MW	HW
Rough.	R	R	S	R
Flow	D	D	D	D

Tab. 1 - Orientation and geomechanical characteristics of the bedding plane (S0) and joint sets (J1–J3) identified in the investigated survey areas. LEGEND: Bed = bedding; J = joint; Pers. = persistence; Spac. = spacing; Aper. = aperture; NC = non-cohesive; MW = moderately weathered; SW = slightly weathered; HW = highly weathered; R = rough; S = smooth; D = dry

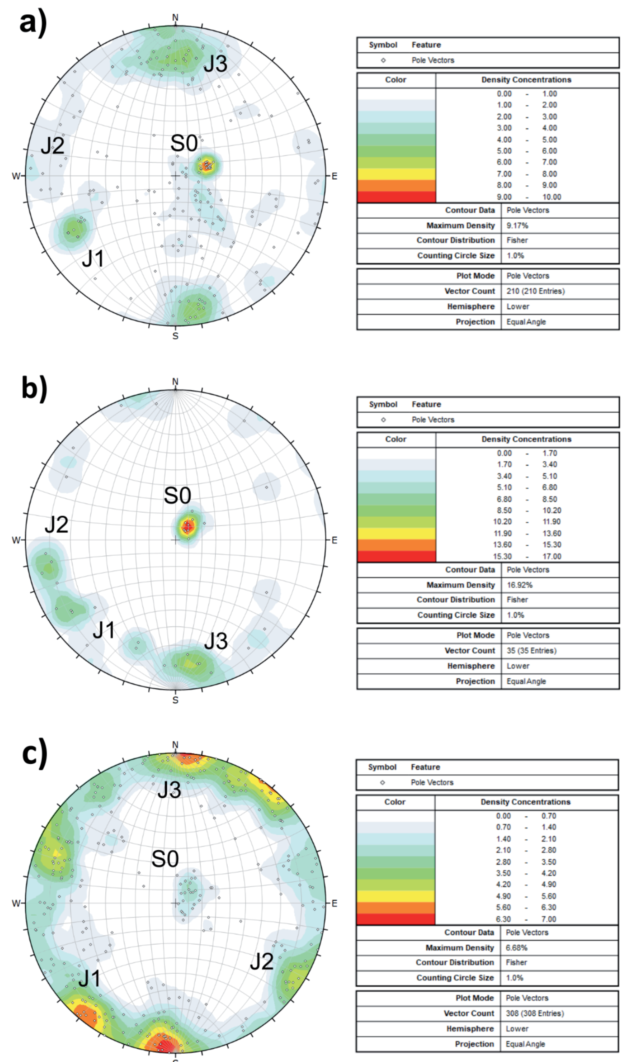

Fig. 4 - Lower-hemisphere, equal-angle stereographic projections of discontinuity poles measured at (a) Poggio Quarry, (b) Riparo dello Speco and (c) Piangrande Cliff

mm (J1) to 3.0 mm (J3). Weathering conditions differ among the joint sets, ranging from slightly weathered surfaces in J1 to highly weathered surfaces in J3, with J2 showing intermediate conditions. Surface roughness is generally high for S0, J1, and J3, whereas smoother surfaces characterize J2. All discontinuity sets are associated with non-cohesive infilling materials and dry conditions, indicating the absence of significant groundwater circulation at the time of investigation.

The SMR classification was applied to the Piangrande Cliff considering two slope orientations (Sector 1: 72/005 and Sector 2: 72/064). The results, summarized in Table 2, are identical for both sectors and indicate rock mass conditions ranging from good (Class II) to moderate (Class III). Most discontinuity sets (S0, J1 and J2) show good and stable conditions (SMR > 60), suggesting a limited instability potential mainly associated with the failure of isolated blocks. In contrast, the J3 discontinuity set shows lower SMR values (54–58), corresponding to Class III conditions and indicating a higher susceptibility to composite failure mechanisms involving planar, joint-controlled, and wedge failures.

F	*Set*	*SMR*	*Cl*	*Stab.*	*FM*
PF	*S0*	*66.8*	*II*	*G–S*	*FB*
	J1	*73.2*	*II*	*G–S*	*FB*
	J2	*66.8*	*II*	*G–S*	*FB*
	J3	*58.0*	*III*	*M–PS*	*PJW*
T	*S0*	*70.4*	*II*	*G–S*	*FB*
	J1	*69.4*	*II*	*G–S*	*FB*
	J2	*63.1*	*II*	*G–S*	*FB*
	J3	*54.3*	*III*	*M–PS*	*PJW*

Tab. 2 - SMR classification results for the main discontinuity sets of the Piangrande Cliff considering plane failure (PF) and toppling (T) conditions. Values are identical for both slope orientations (Sector 1: 72/005; Sector 2: 72/064). The table reports SMR values, stability classes, qualitative stability conditions and associated failure mechanisms. F = failure mode (PF = plane failure; T = toppling); Cl = SMR class; Stab. = stability condition (G–S = Good–Stable; M–PS = Moderate–Partially stable); FM = failure mechanism (FB = failure of some blocks; PJW = planes, joints and wedges)

The same two slope orientations adopted for the SMR classification were then used for the kinematic analysis (Table 3, Fig. 5). This was performed using DIPS software considering a uniform friction angle of 35°.

F	*Set*	*SMR*	*Cl*	*Stab.*	*FM*
PF	S0	66.8	II	*G–S*	*FB*
	J1	73.2	II	*G–S*	*FB*
	J2	66.8	II	*G–S*	*FB*
	J3	58	III	M–PS	PJW
T	S0	70.4	II	*G–S*	*FB*
	J1	69.4	II	*G–S*	*FB*
	J2	63.1	II	*G–S*	*FB*
	J3	54.3	III	M–PS	PJW

Tab. 3 - Summary of kinematic analysis results obtained using DIPS for the Piangrande Cliff considering two slope orientations (72/005 and 72/064). Percentages refer to critical poles or intersections for each failure mechanism. FM = failure mechanism (PS = planar sliding; WS = wedge sliding; DT = direct toppling; FT = flexural toppling); DS = dataset/set; NL = no limits; int. = intersections; R = remarks (VL = very low; L = low; M = moderate; H = high; N–L = negligible to low; Loc = local or sector-specific condition)

For both slope orientations, planar sliding is characterized by very low critical percentages, indicating a negligible kinematic predisposition. For the 72/005 slope, critical poles account for approximately 2.0% of the dataset, increasing slightly when lateral limits are removed. Similar results are obtained for the 72/064 slope, where critical percentages remain below 3% and

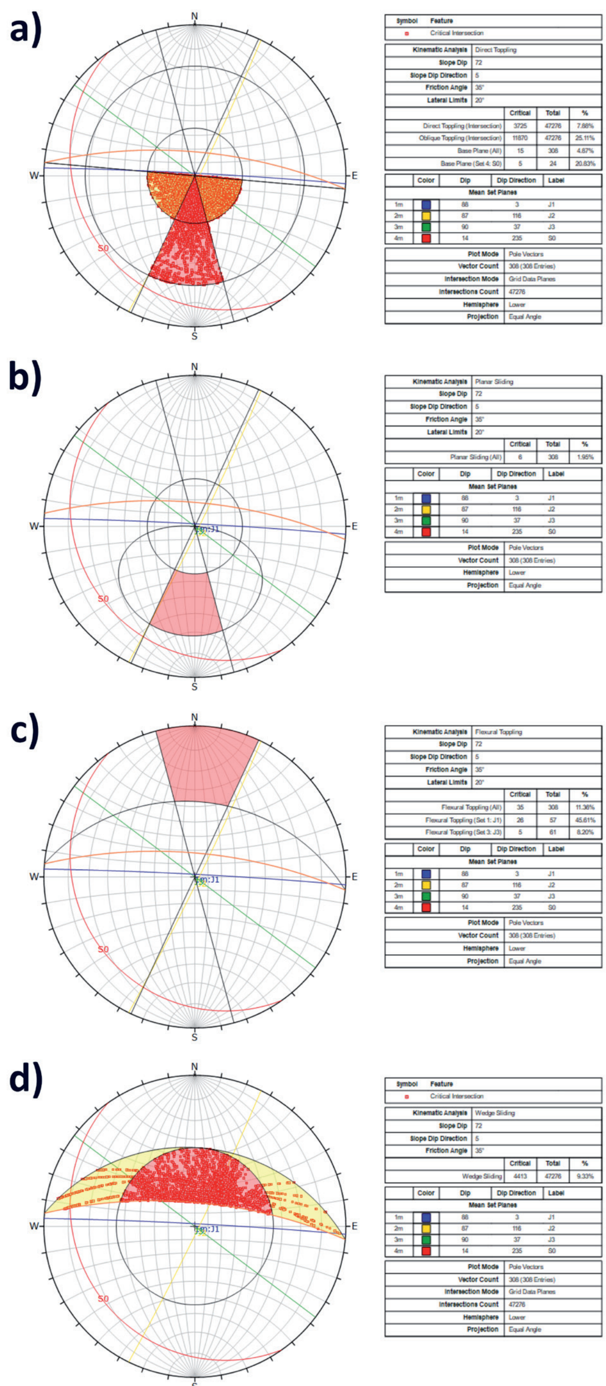

Fig. 5 - *Kinematic analysis results obtained using DIPS for the Piangrande Cliff assuming a friction angle of 35°. Stereographic projections show the kinematic conditions for (a) direct toppling, (b) planar sliding, (c) flexural toppling, and (d) wedge sliding. The diagrams refer to the slope orientation 72/005 and are shown as a representative example of the kinematic analysis performed for the study area*

reach approximately 5.5% only in the absence of lateral constraints. These values confirm that planar sliding is not a dominant instability mechanism under the adopted frictional conditions. Wedge sliding mechanisms show low to very low critical percentages for both slope orientations. For the 72/005 sector, critical intersections are generally negligible, with only local combinations (notably J1–J3) reaching values slightly above 4%. For the 72/064 slope, wedge sliding shows slightly higher critical percentages, with some intersections reaching values of about 6%; however, these remain localized and do not indicate a widespread kinematic susceptibility. Overall, wedge sliding is considered a secondary mechanism for both slope orientations. In contrast, flexural toppling consistently represents the most relevant kinematic mechanism for both slope orientations. For the 72/005 slope, flexural toppling shows moderate critical percentages at the dataset scale (≈11%), with a pronounced contribution from the J1 discontinuity set, for which critical values exceed 45%, identifying it as the dominant kinematic control. For the 72/064 slope, flexural toppling remains significant (≈9% overall), but the contribution is more distributed, with higher values associated with the J3 set (≈18%). This difference indicates a shift in the dominant controlling set between the two slope orientations, reflecting the influence of slope geometry on the kinematic interaction between discontinuities and the cliff face.

Limit equilibrium analysis was carried out on the two 3D models (LiDAR-derived and photogrammetry-derived) using RocSlope3 (Rocscience, 2023). The analysis of the LiDAR-derived model shows that the slope is stable, with all 12,361 blocks generated by the intersection of the slope face and discontinuities displaying high FoS values (all > 3). The photogrammetric-derived model was subdivided by discontinuities into 14,350 blocks. Out of these, 321 have FoS between 3 and 4. Three blocks exhibit FoS below 1. Figure 6 shows an example of the limit equilibrium analysis performed on the photogrammetry-derived model.

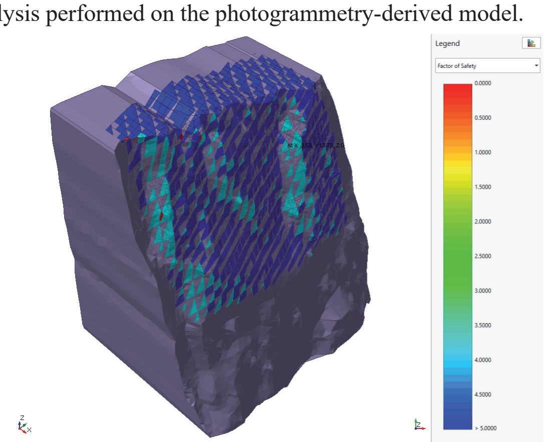

Fig. 6 - *RocSlope3 limit equilibrium analysis of the first portion of the photogrammetry-derived model. The factor of safety is greater than 5 for most of the outcrop; two blocks are identified as falling, with FoS = 0, whereas the remaining blocks affected by sliding show FoS values greater than 3*

Numerical modelling was also carried out on sections extracted from both the photogrammetry-derived and LiDAR-derived models. To facilitate the computational process, the analysis was performed along 2D sections extracted from the two models.

The results for the LiDAR-derived model indicate an overall stability, with no blocks showing sliding or failure. In contrast, the simulation performed on the photogrammetry-derived section highlights the instability of small blocks (Figure 7). These blocks are located in a portion of the slope characterized by overhanging geometry, which was not captured in the LiDAR-derived profile.

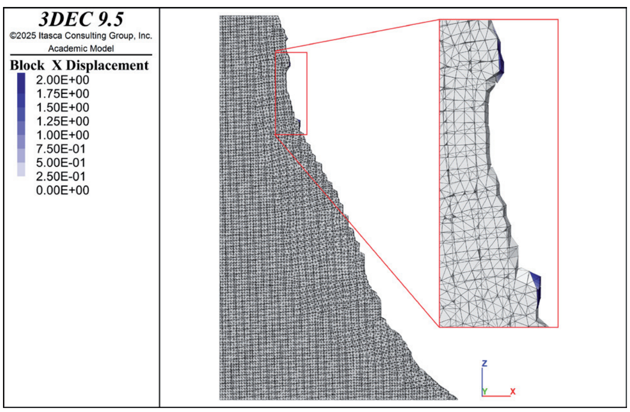

Fig. 7 - 3DEC numerical simulation of a section extracted from the photogrammetry-derived model. The results highlight the instability of small blocks located in the overhanging portion of the slope

DISCUSSION

The integrated methodological approach adopted in this study demonstrates that the stability of the Piangrande Cliff is primarily controlled by its structural configuration and by the geometric relationships between discontinuity sets and slope orientation. The combined use of remote sensing techniques and traditional field surveys allowed the acquisition of high-quality structural and geomorphological data in sectors that would otherwise be inaccessible or unsafe to investigate, confirming the crucial role of these technologies in modern coastal cliff studies.

The identification of a gently dipping bedding plane (S0) associated with multiple steeply dipping joint sets (J1–J3) defines a structurally complex rock mass, predisposed to the development of kinematically controlled instability mechanisms.

This framework is consistent with previous studies (Mammoliti *et alii*, 2022; Fullin *et alii*, 2023) conducted along the Conero coastal sector and supports the interpretation of a regionally persistent discontinuity pattern, locally modified by outcrop-scale deformation and exposure conditions.

Geomechanical characterization and SMR classification provided a first-order assessment of rock mass quality and stability. The SMR shows that the rock mass quality varies from good to moderate. These conditions suggest a limited potential for instability, mainly restricted to the failure of isolated blocks.

Kinematic analyses, performed using the Markland stereographic method as implemented in DIPS, further refined the interpretation by evaluating the geometric admissibility of potential failure mechanisms. In agreement with the SMR classification, the kinematic analysis highlighted that the probability of planar and wedge sliding is low, indicating a limited kinematic predisposition to failure. However, unlike the geomechanical classification alone, the kinematic analysis also shows that flexural toppling represents the most critical potential failure mechanism. This difference reflects one of the limitations of the SMR classification, which does not account for flexural toppling. Furthermore, it should be emphasized that the SMR classification was based on the mean orientation of the main discontinuity sets, whereas the DIPS kinematic analysis considered all measured discontinuities within the rock mass. Regarding the limit equilibrium and numerical analyses, these were performed using both UAV-photogrammetric and LiDAR-derived models. The limit equilibrium analysis highlighted stable conditions when the LiDAR-derived model was used and identified some unstable blocks when the photogrammetry-derived model was used. This difference is related to the different acquisition geometry between the two surveys. The oblique and frontal image acquisition geometry adopted during the photogrammetric survey allowed for capturing more details in the sub-vertical Piangrande slope face, including some overhanging sections. These overhanging sections played an important role in the kinematics of block failures and therefore reduced the FoS. A similar behaviour emerges in the numerical simulation carried out with the discontinuum code 3DEC. Also in this case, when using the 3D model extracted from the LiDAR survey, the slope appears to be stable, while when using the photogrammetric model, the analysis clearly shows some blocks failing along the overhanging section.

In this case, both limit equilibrium and numerical modelling indicate a high likelihood of block failure in the steepest, locally overhanging portions of the slope. However, a detailed geological and geomorphological interpretation of the slope and past failures suggests that two types of potential failures may occur. The first, as indicated by limit equilibrium and numerical modelling, is associated with a single rock block failing from an overhanging section. The second is associated with fracture propagation and progressive failure, potentially leading to larger rockfalls. A schematic example of such failures is represented in Figure 8, where the two different failure mechanisms can be observed: a smaller failure associated with overhanging geometry, and a larger slope failure related to fracture propagation and progressive failures.

In light of this, none of the stability models adopted in this study appears able to reproduce large progressive failures, instead highlighting only single rockfalls associated with overhanging geometry. An exhaustive geomorphological and geological interpretation, also supported by remote sensing techniques, may improve the interpretation of slope stability results and enhance understanding of their limitations. In this context, recent advances in visualization methods may represent an important tool for improved geological and geotechnical interpretation. An example of this is the use of virtual and augmented reality (VR/AR). Figure 9 shows an example of the application of this technique in the Conero Regional Park, highlighting its potential for hazard assessment and risk mitigation strategies.

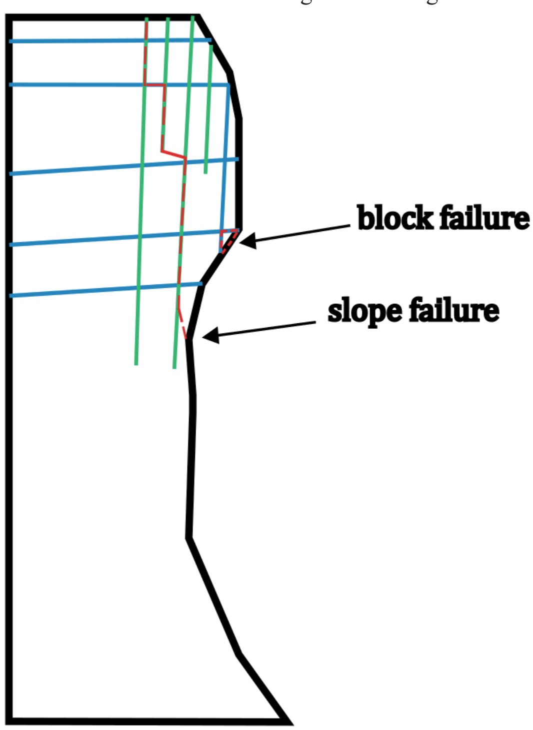

Fig. 8 - The two different failure mechanisms at the Piangrande slope: a smaller failure associated with overhanging geometry and a larger slope failure related to fracture propagation and progressive failure

CONCLUSIONS

This study demonstrates the importance of integrating high-resolution remote sensing data with conventional and numerical stability analyses for the investigation of structurally complex coastal rock slopes. UAV-based photogrammetric surveys proved particularly valuable for reconstructing detailed slope geometries and discontinuity networks in steep and inaccessible sectors, providing a level of geometric realism that cannot be achieved through traditional field surveys.

The structural setting of the Monte Conero coastal cliff is dominated by a gently dipping bedding plane combined with three steeply dipping joint sets, consistent with the regional tectonic framework.

Fig. 9 - Augmented reality visualization of a 3D model of Conero Regional Park

Geological and geomorphological interpretation of the UAV data suggests that past failures may be associated with two main mechanisms: single-block failures in steep or overhanging sectors, and larger failures related to progressive fracture propagation.

Geomechanical classification indicates good to moderate rock mass conditions. Similarly, kinematic analyses indicate overall slope stability, with flexural toppling representing the most relevant potential failure mechanism, although with relatively low critical percentages. These results are only partially consistent with the geological and geomorphological interpretation, reflecting the inherent limitations of the two methods, as discussed above.

Limit equilibrium and numerical analyses indicate globally stable conditions when the LiDAR-derived model is used. In contrast, when the photogrammetry-derived model is adopted, the analyses indicate the possibility of block failure in the steepest and locally overhanging portions of the slope, in agreement with the geological and geomorphological interpretation. This demonstrates the importance of reconstructing accurate slope geometries in complex structural settings.

It is however important to note that none of the methods used were able to reproduce the larger slope failure associated with fracture propagation mechanisms. Reproducing such failure mechanisms is more complex and can be done only through hybrid numerical codes (FEM-DEM, Finite Element and Discrete Elements methods).

Therefore, any reliable stability analysis must be grounded in a thorough geological and geomorphological interpretation. Only on this basis is it possible to understand the strengths and limitations of the adopted methods and to interpret the results correctly.

Funding

Funded by Interreg Italy-Croatia Programme 2021–27, 1st call for proposals, standard project proposal. Project: RESONANCE (impRoving landslidE riSk preventiOn aNd mAnagement iN Coastal arEas), and by European Union – Next Generation EU. Project PRIN 2022: Progetti di Ricerca di Rilevante Interesse Nazionale – Bando 2022. Prot. 2022B3ZFSR. P.I.: Mirko Francioni, University of Urbino, Carlo Bo.

REFERENCES

Agliardi F., Riva F., Barbarano M., Zanchetta S., Scotti R. & Zanchi A. (2019) - *Effects of tectonic structures and long-term seismicity on paraglacial giant slope deformations: Piz Dora (Switzerland)*. Engineering Geology, **263**: 105353. https://doi.org/10.1016/j.enggeo.2019.105353

Atencio E., Muñoz A., Lozano F., González-Arteaga J. & Lozano-Galant J.A. (2024) - *Calibration of iPad Pro LiDAR scanning parameters for the scanning of heritage structures using orthogonal arrays*. Applied Sciences, **14**: 11814. https://doi.org/10.3390/app142411814

Calamita F., Coltorti M., Pierucci P. & Pizzi A. (1999) - *Evoluzione strutturale e morfogenesi plio-quaternaria dell'Appennino Umbro-Marchigiano tra il Pedappennino Umbro e la costa adriatica*. Bollettino della Società Geologica Italiana, **118**: 125-139.

Cello G. & Coppola L. (1989) - *Modalità e stili deformativi nell'area anconetana.* Studi Geologici Camerti, **XI**: 37-48.

Coltorti M. & Sarti M. (2011) - *Note illustrative della Carta Geologica d'Italia alla scala 1:50.000, Foglio 293 - Osimo*. Progetto CARG, ISPRA - Servizio Geologico d'Italia.

Esposito G., Salvini R., Matano F., Sacchi M., Danzi M., Somma R. & Troise C. (2017) - *Multitemporal monitoring of a coastal landslide through SfM-derived point cloud comparison*. The Photogrammetric Record, **32**: 459-479.

Fan W., Lv J., Cao Y., Shen M., Deng L.& Wei Y. (2019) - *Characteristics and block kinematics of a fault-related landslide in the Qinba Mountains, western China.* Engineering Geology, **249**: 162-171. https://doi.org/10.1016/j.enggeo.2018.12.019

Feliziani F., Marmoni G. M. ,Istrati D. , GianniV. , Bozzano F. & Martino S. (2024) - *Stability analysis of sea-cliffs coupling stress strain and hydrodynamic modelling as a tool for modern archeological site preservation strategies.* EGU General Assembly 2024, Vienna, Austria, 14-19 Apr 2024, EGU24-585. https://doi.org/10.5194/egusphere-egu24-585, 2024.

Fullin N., Duo E., Fabbri S., Francioni M., Ghirotti M. & Ciavola P. (2023) - *Quantitative characterization of coastal cliff retreat and landslide processes at Portonovo–Trave cliffs (Conero, Ancona, Italy) using multi-source remote sensing data*. Remote Sensing, **15**: 4120. https://doi.org/10.3390/rs15174120

Guerriero L., Annibali Corona M., Di Martire D., Francioni M., Limongiello M., Tufano R. & Calcaterra D. (2024) - *Rockfall susceptibility analysis of the "San Michele Arcangelo" historic trail (Central Italy) based on virtual outcrops and multiple propagation models.* Bulletin of Engineering Geology and the Environment, **83**: 263. https://doi.org/10.1007/s10064-024-03713-0

International Society for Rock Mechanics Commission on Standardization of Laboratory and Field Tests (1978) - *Suggested methods for the quantitative description of discontinuities in rock masses.* International Journal of Rock Mechanics and Mining Sciences & Geomechanics Abstracts, **15**: 319-368.

Łabędź P., Skabek K., Ozimek P., Rola D., Ozimek A. & Ostrowska K. (2022) - *Accuracy verification of surface models of architectural objects from the iPad LiDAR in the context of photogrammetry methods*. Sensors, **22**: 8504.

Mammoliti E., Fronzi D., Cambi C., Mirabella F., Cardellini C., Patacchiola E., Tazioli A., Caliro S. & Valigi D. (2022) - *A holistic approach to study groundwater–surface water modifications induced by strong earthquakes: The case of Campiano catchment (Central Italy)*. Hydrology, **9**: 97.

Mandaglio M.C. (2024) - *Geomechanical characterization of the rock mass along a deep vertical borehole.* Geotechnics, **4**: 209-228.

Martin S., Fedrizzi F., Boaga J., Cenni N., Agnini C., Cortellazzo G. & Rossato S. (2020) - *Paleo-seismicity in the Euganean Hills Province (Northeast Italy): constraints from geomechanical and geophysical tests in the Schio–Vicenza fault area*. Frontiers in Earth Science, **8**: 586897

Montanari A., Mainiero M., Coccioni R. & Pignocchi G. (2016) - *Catastrophic landslide of Medieval Portonovo (Ancona, Italy).* Geological Society of America Bulletin, **128**: 1660-1678.

Neuman Shlomo P. (2005) - *Trends, prospects and challenges in quantifying flow and transport through fractured rocks.* Hydrogeology Journal, **13**: 124-147.

Pierantoni P., Deiana G. & Galdenzi S. (2013) - *Stratigraphic and structural features of the Sibillini Mountains (Umbria–Marche Apennines, Italy).* Italian Journal of Geosciences, **132**: 497-520.

Weidinger J.T., Korup O., Munack H., Altenberger U., Dunning S.A., Tippelt G. & Lottermoser W. (2014) - *Giant rockslides from the insid*e. Earth and Planetary Science Letters, **389**: 62-73.

Westoby M.J., Brasington J., Glasser N.F., Hambrey M.J. & Reynolds J.M. (2012) – *Structure-from-Motion photogrammetry: A low-cost, effective tool for geoscience applications.* Geomorphology, **179**: 300-314.

Williams A. & Pranzini E. (2018) - *Rock coasts.* In Encyclopedia of Coastal Science; Springer: Berlin/Heidelberg, Germany.

Young A.P. & Carilli J.E. (2019) - *Global distribution of coastal cliffs.* Earth Surface Processes and Landforms, **44**: 1309-1316.

Softwares

Agisoft (2025) - *Agisoft Metashape*. Available online: http://www.agisoft.com/downloads/installer/

Cloudcompare Team (2025) - *CloudCompare tools: Compass mode* - extracting structural measurements.

DJI (2024) - *DJI Terra* (Version 4.0). Shenzhen, China: DJI Technology Co., Ltd. Available online: https://www.dji.com/dji-terra

Girardeau-Montaut D. (2016) - *CloudCompare* (version 2.10). Available online: http://www.cloudcompare.org

Itasca Consulting Group, INC. (2023) - *3DEC-Three-dimensional distinct element code* (Version 9.6). Minneapolis, MN, USA. Available online: https://www.itascacg.com/software/3dec

MathWorks (2025) - *MATLAB* (Version R2025a). Natick, MA, USA: The MathWorks Inc.

RocScience INC. (2023) - *RocSlope3-Three-dimensional limit equilibrium analysis for slopes* (Version 1.0).
Toronto, ON, Canada. Available online: https://www.rocscience.com/software/rocslope3

Robert McNeel & Associates (2024) - *Rhinoceros* (Version 8). Seattle, WA, USA: Robert McNeel & Associates.

Received January 2026 - Accepted March 2026